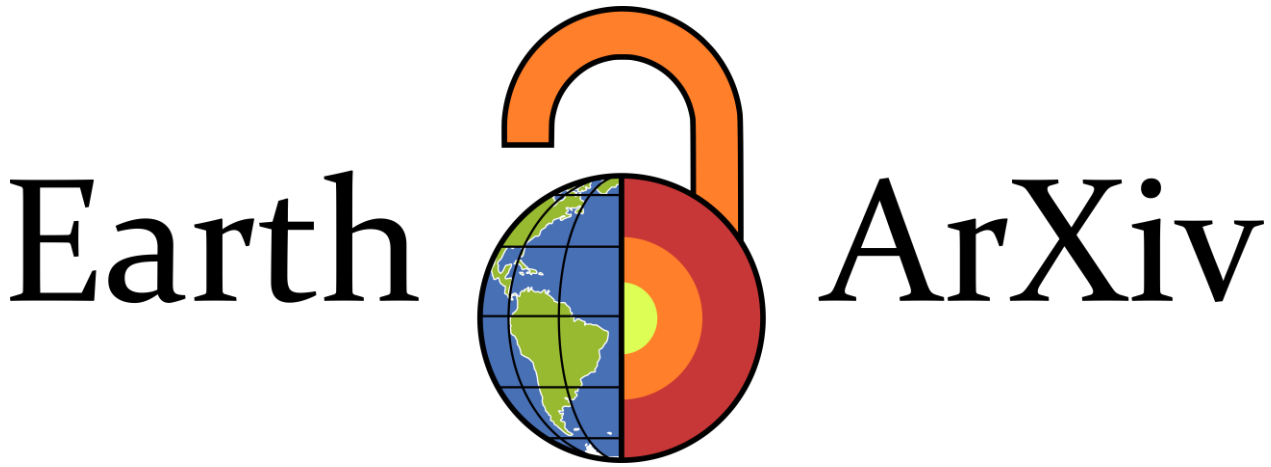

We are still deciding which journal the manuscript will be submitted to. Please note the manuscript has yet to be formally accepted for publication. Subsequent versions of this manuscript may have slightly different content. If accepted, the final version of this manuscript will be available via the 'Peer-reviewed Publication DOI' link on the right-hand side of this webpage. Please feel free to contact any of the authors; we welcome feedback.

Transformer Assisted UNet for Marine Litter Detection on Sentinel-2 Imagery

Abstract

The contamination of marine environments with man-made litter is a growing nation-wide concern. Satellite imagery combined with deep learning–based detection models has emerged as a robust and cost-effective solution for large-scale marine litter monitoring. In this article, we present a novel deep learning-based scheme to detect marine litter using Sentinel-2 imagery based on the Deep UNet architecture, introducing self- and cross-attention mechanisms into the decoder via transformer layers. The model leverages all Sentinel-2 bands except B10, and the NDVI and FDI indices are additionally incorporated to better guide the segmentation process. To evaluate the proposed method, we train it on the FloatingObjects dataset, a widely used benchmark for marine debris detection, and the results show that it compares favorably against state-of-the-art approaches.

Keywords: Marine Litter, Plastics, Detection, Sentinel-2, UNet, Transformers

1 Introduction

Marine litter is increasingly common along coastlines, where items such as bags, food wrappings, and tin cans are frequently found. While this litter is heterogeneous, about 80% of man-made items entering marine environments are plastics (Morales-Caselles et al. 2021). The contamination of marine ecosystems with large quantities of plastics and microplastics has escalated rapidly over recent decades (Löhr et al. 2017), becoming a global environmental, health, and socioeconomic concern (Wayman and Niemann 2021; Galgani et al. 2021). The fundamental issue with this type of contamination lies in its persistence, as the degradation process is extremely slow (Andrady 2015). As a result, plastic pollution generates a wide range of impacts: harm to marine wildlife (Soto-Navarro et al. 2021; Woods et al. 2021), risks to human health (Aretoulaki et al. 2021), and substantial economic costs, including prevention, damage to equipment and commercial stocks, remediation, and the broader consequences of inaction (Mafuta et al. 2021; McIlgorm et al. 2022).

Globally, the density of floating debris ranges from nearly 0 to over 600 items per km^2 (Galgani et al. 2015), a variability that makes the detection of small residues particularly difficult. Traditional monitoring relies on ship-based visual surveys, which

require substantial human and financial resources (Salgado-Hernanz et al. 2021), or on numerical models, which may lack sufficient accuracy (Topouzelis et al. 2021).

Recent efforts have explored the use of unmanned aerial vehicles (UAVs) and satellite imagery for detecting marine litter. UAVs provide very high spatial resolution but scale poorly across large regions or long time periods. In contrast, satellite missions such as Sentinel-2 (S2) (European Space Agency 2025) offer global coverage and a high revisit frequency, despite their low to medium spatial resolution (up to 10 m for S2). Importantly, plastics exhibit distinctive spectral signatures in the near-infrared (NIR) and short-wave infrared (SWIR) regions (Biermann et al. 2020), which can be effectively captured by sensors such as those on S2 (Kikaki et al. 2022). These observations have spurred the development of satellite-only marine litter detection methods. While several classical machine-learning models have been proposed (Biermann et al. 2020; Sannigrahi et al. 2022), deep learning approaches remain the most promising (Mifdal et al. 2021; Jamali and Mahdianpari 2021).

In this article, we propose a deep-learning, end-to-end semantic segmentation model for detecting marine litter using S2 imagery. The model builds upon a Deep UNet architecture (Li et al. 2018) and extends the work by Costa et al. (Costa et al. 2024). Our primary contribution lies in integrating a transformer layer into the UNet decoder, enhancing the model's ability to capture long-range dependencies. To evaluate the proposed method, we train it on the FloatingObjects dataset (Mifdal et al. 2021; Carmo et al. 2021), a widely used benchmark for marine debris detection, and compare its performance against state-of-the-art approaches.

The remainder of the paper is organized as follows. Section 2 provides a comprehensive review of recent work on S2-based marine litter detection and deep-learning segmentation. Section 3 describes the dataset and the implementation details of the proposed model. Section 4 presents a detailed performance analysis, including qualitative and quantitative comparisons and an ablation study exploring different model configurations. Section 5 discusses the results and outlines directions for future research, and Section 6 summarizes the main conclusions.

2 Related Work

The traditional marine litter detection and monitoring approach involves human expeditions conducted at different times and locations, in which floating litter is visually identified and subsequently sampled to study its properties (Salgado-Hernanz et al. 2021). Although simple and effective, this method is not efficient, and its reliance on human labor introduces several limitations. The requirement for personnel to remain constantly vigilant for floating debris is often impractical and costly (Yang et al. 2024). To reduce the dependence on manual observation, some alternatives have been proposed, such as installing multiple motion cameras on the bows of fishing vessels (De Vries et al. 2021; Yang et al. 2024). These cameras produce photo time-lapses at intervals of a few seconds, resulting in near-continuous data from the surveyed region. However, human involvement is still necessary for data collection, and the acquired images must be further processed to analyze the quantity and type of plastics present.

We remark that traditional methods are usually complemented with the use of numerical simulations, specifically Lagrangian models to study the trajectories of marine litter and possible accumulation hotspots (Carlson et al. 2017; Mansui et al. 2020). Still, the complexity of modeling particle behavior and the high amount of phenomena which should be accounted for can lead to erroneous estimations.

To overcome these limitations, considerable research has focused on detection and monitoring using UAVs and satellite imagery. On one hand, UAV-based missions are less intrusive than boat expeditions and do not disturb the marine ecosystem (Merlino et al. 2021; Escobar-Sánchez et al. 2022). Drone-acquired data is usually georeferenced, allowing for more precise detection of plastics and the identification of potential accumulation zones (Merlino et al. 2021). Nevertheless, despite the growing accessibility of UAV technology, no standardized processing pipeline exists for analyzing drone imagery. Image processing methods often vary according to project-specific goals, making it difficult to establish a unified framework for UAV-based marine debris detection (Merlino et al. 2020).

On the other hand, satellite data, despite its lower resolution, offers the advantage of providing long-term observations over extensive areas without the need for direct human intervention. Satellite sensors have proven highly valuable for plastic detection. Topouzelis et al. (Topouzelis et al. 2019) showed that the detection of certain types of plastics requires multi- and hyperspectral imagery, as their reflectance is easily detected in the NIR wavelengths. Several satellites have been employed in the literature to detect and study marine litter, such as WorldView-3, used to observe plastics in the Great Pacific Garbage Patch (Park et al. 2021); PRISMA, applied to study the Greek island of Lesvos (Taggio et al. 2022); and Sentinel-2, which has been widely used in different scenarios (Topouzelis et al. 2019; Themistocleous et al. 2020; Ciappa 2021).

2.1 Sentinel-2 Marine Litter Detection

The Sentinel-2 (S2) mission, part of the Copernicus program of the European Space Agency (ESA), is particularly attractive due to its high spatial resolution when compared to other satellites and the open-access policy of the program. The mission consists of two twin satellites orbiting the Earth, providing a 5-day revisit cycle at the equator (European Space Agency 2025). S2 satellites acquire imagery in 13 spectral bands: four at 10 m resolution, covering the visible and NIR spectrum; six at 20 m resolution, including several within the SWIR range; and three additional bands at 60 m resolution—see Figure 1. While the coarser bands provide less spatial detail, they capture unique spectral information that can be highly valuable for specific applications.

One of the first studies to investigate the use of S2 imagery for marine litter detection is (Topouzelis et al. 2019). Serving primarily as a proof of concept, the study combines unmanned aerial systems with S2 imagery to detect artificially deployed floating plastic targets. The detection is performed manually, with an emphasis on identifying the wavelengths that best highlight the targets.

Subsequent studies incorporate detection algorithms to automate the task. Some employ classical methods, such as (Topouzelis et al. 2020), which applies a spectral signature detection procedure that extracts plastic target signatures through inverse

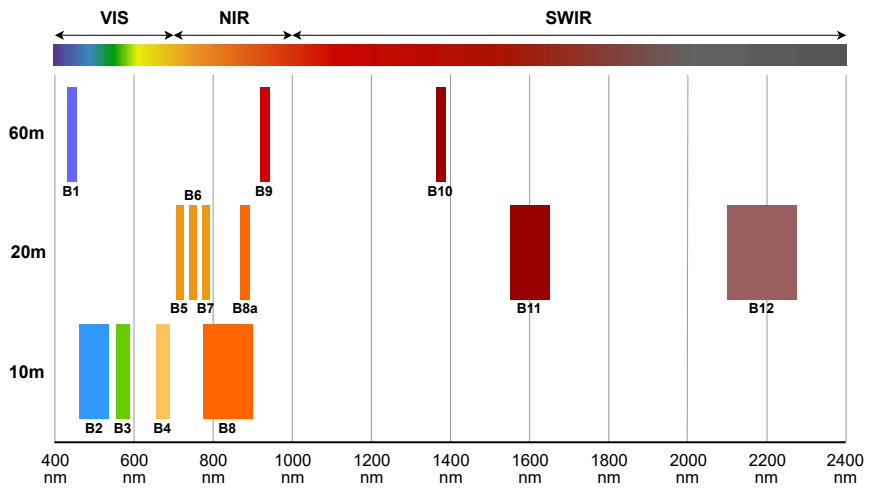

Fig. 1: Distribution of the Sentinel-2 bands across the wavelength spectrum.

spectral unmixing followed by matched filtering on S2 imagery, and others adopt machine learning techniques. Among the latter, Biermann et al. (Biermann et al. 2020) introduce the Floating Debris Index (FDI) and use it, together with the Normalized Difference Vegetation Index (NDVI) and remote sensing reflectance values from S2 imagery, as inputs to a Naive Bayes classifier in order to assign pixels to different material classes—water, seaweed, timber, plastic, foam, and pumice. In (Basu et al. 2021), the authors evaluate the floating plastic detection performance of two unsupervised (K-means and fuzzy c-means) and two supervised (support vector regression (SVR) and semi-supervised fuzzy c-means) classification algorithms, concluding that the supervised ones, especially SVR, achieve the best results. Similarly, (Sannigrahi et al. 2022) compare the effectiveness of SVR and Random Forest (RF) for the same task using different combinations of S2 bands and spectral indices as inputs. More recently, in (Nivedita et al. 2024), the authors expand on the work of Biermann et al. by using the NDVI together with the FDI and selected S2 reflectances to derive spectral fingerprints. These features are then fed into a Naive Bayes classifier to categorize pixels into the same material classes.

The use of deep learning-based schemes for marine debris detection using S2 imagery has also been explored. For example, (Mifdal et al. 2021) trains and evaluates a UNet convolutional neural network (Li et al. 2018) to classify the pixels of S2 imagery into five material classes, matching those defined in (Biermann et al. 2020). In (Jamali and Mahdianpari 2021), a deep learning-based Generative Adversarial Network-Random Forest is shown to outperform the traditional machine learning algorithms RF and SVR for large-scale marine pollution detection using S2 imagery. Gómez et al. (Gómez et al. 2022) focus on detecting plastic debris in rivers by adapting the image segmentation procedures UNet and DeeplabV3+ (Chen et al. 2017) to the S2

setting. Similarly, the authors of (Rußwurm et al. 2023) perform marine debris detection using the aforementioned segmentation scheme UNet and an enhanced version, UNet++, that replaces the encoder by a residual-network feature extractor.

2.2 Attention Mechanisms in Remote Sensing Image Segmentation

In recent years, semantic segmentation networks have incorporated attention mechanisms (Fan et al. 2020; Zhao et al. 2023; Liu et al. 2024; Kikaki et al. 2024) to extract the main features, relying on the fact that attention mimics the human eye: it ignores irrelevant parts of the image to focus on the main characteristics. From a quantitative point of view, architectures with attention modules have been proven to be more accurate (Ruan et al. 2022).

In particular, we highlight the increasing use of attention mechanisms in remote sensing segmentation networks. Li et al. (Li et al. 2020) combine a channel attention module, to learn the relationships between channels, with a spatial attention one to aggregate spatial information, which is useful when detecting smaller objects. Cui et al. (Cui et al. 2023) introduce channel attention and residual modules in the encoder, a multi-feature fusion mechanism in the decoder, and improved sub-pixel convolution for upsampling, achieving superior accuracy and efficiency in remote sensing semantic segmentation compared to UNet and other baselines.

Ben Salah et al. (Ben Salah et al. 2025) introduce a multi-head attention mechanism (Vaswani et al. 2017) to improve the spatial details of roads and paths. This architecture consists of several parallel self-attention operations called heads, allowing models to jointly attend to information from different positions. Others, such as Liu et al. (Liu et al. 2024) rely on transformer-based architectures. They propose building a segmentation network using channel and spatial attention blocks after each U-shaped residual block to make up the encoder and decoder. Channel attention allows the network to emphasize the most important feature channels, while spatial attention can focus on the most relevant regions. These attention mechanisms are combined with a Swin Transformer with two multi-head self-attention modules installed at the skip-connections. The Swin Transformers were previously used by Cheng et al. (Cheng et al. 2022) to develop *Mask2Former*, which incorporates a pixel decoder to upsample the low-resolution features produced by the encoder, along with a transformer decoder that generates object queries from the image features. The final segmentation mask is then obtained by decoding these object queries into per-pixel embeddings.

3 Materials and Methods

Our proposed workflow, depicted in Figure 2, consists of a training phase, an evaluation phase, and a quality assessment. During the training phase, we select preprocessed data from the FloatingObjects dataset, choose the desired bands, compute the FDI and NDVI, and feed them into the proposed neural network in order to train it. Once the network is trained, we move on to the evaluation stage, where preprocessed data from the area of interest is fed into the network to obtain a binary mask indicating the

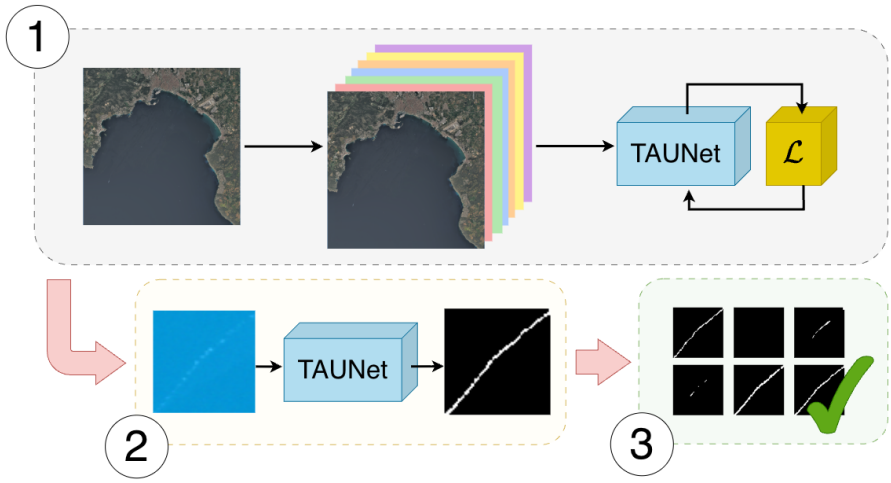

Fig. 2: Workflow of the proposed method. In (1), preprocessed data from the FloatingObjects dataset is used to train TAUNet (see Figure 3 for the full network architecture) with selected spectral bands and indices (FDI, NDVI). In (2), the trained model is applied to the area of interest to produce binary masks of floating debris. Finally, in (3), we perform qualitative and quantitative evaluation.

location of predicted floating debris. Finally, we perform a quality assessment, both by visual examination and by quantitative comparison.

3.1 Training data

We train our model on the FloatingObjects dataset, first introduced in (Mifdal et al. 2021) and later expanded in (Rußwurm et al. 2023) . This hand-annotated dataset is specifically designed for remote sensing applications involving floating-object detection. It comprises 26 globally distributed Sentinel-2 coastal scenes, each provided with pixel-level binary masks distinguishing floating from non-floating objects. All spectral bands have been preprocessed and upscaled to a spatial resolution of 10 m.

The dataset exhibits substantial geographical and environmental variability, spanning diverse coastal conditions, water types, illumination scenarios, and object appearances. However, despite this variability, its overall size remains relatively limited, both in the number of scenes and in the total amount of annotated pixels. As a result, the use of deep learning models must be approached with caution, as the dataset may not fully support large-capacity networks without risk of overfitting.

We consider as inputs to our model all Sentinel-2 bands except B10, which is mainly used for cirrus cloud detection and does not contain much surface information (European Space Agency 2025). Additionally, we follow the common strategy in satellite-based object detection of considering spectral indices as additional inputs. Even though the indices are computed using the bands which are already fed into the model, it has been argued that this addition better guides the detection of specific

materials and increases performance (Mifdal et al. 2021). In our case, we use the most widely used indices in the floating marine debris detection setting: FDI and NDVI.

The Floating Debris Index (FDI) introduced in (Biermann et al. 2020), was specifically designed for marine litter detection. Its precise formula in terms of S2 bands is

$$\mathrm{FDI} = B8 - \left(B6 + (B11 - B6) \cdot \frac{\lambda_{B8} - \lambda_{B6}}{\lambda_{B11} - \lambda_{B6}} \right), \tag{1}$$

where here and throughout this subsection Bn denotes the corresponding S2 band and λ_{Bn} its central wavelength—in practice, $\lambda_{B6} = 740, \lambda_{B8} = 842$, and $\lambda_{B11} = 1610$. We interpret the index as the subtraction of the actual NIR reflectance ($B8$) and the expected NIR reflectance, which is estimated by linear interpolation between the red edge ($B6$) and SWIR ($B11$) bands. This way, FDI measures anomalous NIR reflectance values, which should highlight floating debris, as both plastic and organic material reflect much more NIR than water.

The FDI is often paired with the Normalized Difference Vegetation Index (NDVI), which in a marine context is used for detecting patches of algae and other plant material. This index helps to differentiate floating debris and vegetation patches, reducing false positives (Biermann et al. 2020). In terms of S2 bands, the NDVI reads as

$$\mathrm{NDVI} = \frac{B8 - B4}{B8 + B4}.$$

For model development, the bands and indices corresponding to each scene are cropped into patches of size 64×64, which are then split into training and test subsets using an 80%-20% ratio.

3.2 Marine debris detector implementation

We propose an end-to-end data-driven semantic segmentation method for marine litter detection on S2 imagery. The model is based on a Deep UNet architecture (Li et al. 2018) and follows an encoder–decoder structure with skip-connections. The decoder incorporates Transformer Layers to enhance the extraction of relevant features for marine litter segmentation. The complete architecture of our *Transformer Assisted UNet* (TAUNet from now on) is shown in Figure 3a. We remark that even though Transformers were proposed by Vasawani et al. (Vaswani et al. 2017) for language models, in this model we use the Video Transformer architecture presented by Dosovitskiy et al. (Dosovitskiy 2020). To reduce the computational cost of the algorithm, they propose to split the image into non-overlapping patches, each of which is flattened and linearly projected into a patch embedding that serves as an input token to the transformer encoder. In our case, we apply the patch-based tokenization to the feature maps produced by the UNet. Each patch represents a local region in the feature space and is used as a token input to the transformer-based attention module.

The encoder path follows the design of (Li et al. 2018; Costa et al. 2024) with three resolution levels. At the lowest level, the feature map is passed through a Transformer Layer with self-attention, illustrated in Figure 3b, where both keys and queries are copies of the same input. Self-attention is used here to capture long-range dependencies

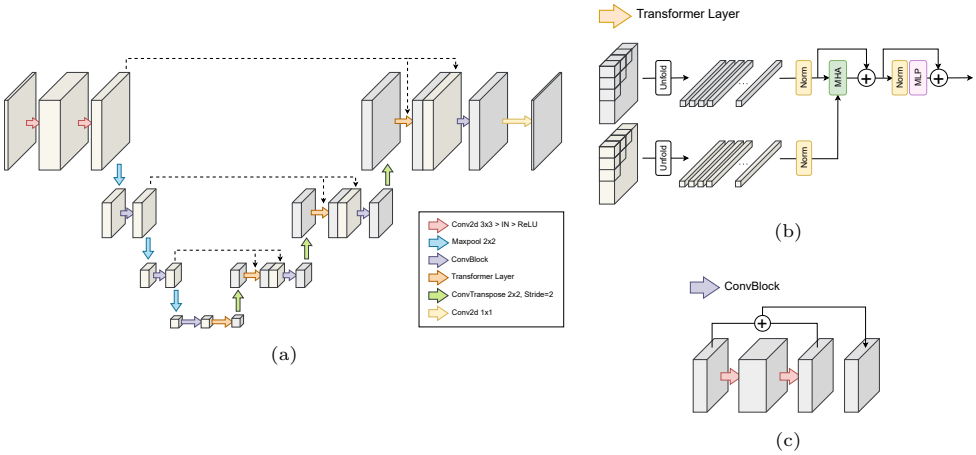

Fig. 3: (a) Overall architecture of the TAUNet. (b) Transformer Layer architecture, with the Multi-Head Attention module (c) Residual convolutional block.

within the same feature map, enabling the network to model relationships between distant regions of the image. In the decoder, the downsampled features from the encoder are used twice at each level: first, as keys and queries for the Transformer Layer operating on the upsampled feature map with cross-attention; and second, concatenated with the output of this Transformer Layer. Cross-attention allows the decoder to integrate information from the encoder features while refining the upsampled representation, thereby enhancing the reconstruction of fine details. The subsequent upsampling blocks follow the design of Costa et al. (Costa et al. 2024).

Normalization layers are included throughout the network to improve training stability. We employ Instance Normalization (IN) (Topouzelis et al. 2020), which rescales and recenters each image in a mini-batch independently. Unlike Batch Normalization (BN) (Ioffe and Szegedy 2015), IN computes mean and variance dynamically during inference, making it more suitable for this task due to the strong variability observed in floating object regions.

Finally, following (Costa et al. 2024), the binary segmentation mask M, which indicates the presence or absence of floating objects, is obtained from the multispectral image together with NDVI and FDI. The output of the TAUNet is passed through an exponential activation function and then thresholded at 0.3 to produce the final mask.

3.3 Training details

To train the proposed model we employ a combination of two metrics commonly used for semantic segmentation. In particular, it is defined as

$$\mathcal{L} := \mathcal{L}_{BCE} + \mathcal{L}_{Dice}, \tag{2}$$

where $\mathcal{L}_{BCE}$ denotes the Binary Cross Entropy (BCE) loss and $\mathcal{L}_{Dice}$ the Dice loss (Jadon 2020). The BCE loss compares the predicted probability $p \in [0, 1]$ with the

ground truth label $y \in \{0, 1\}$, and it is computed as

$$\mathcal{L}_{BCE}(y, p) \coloneqq -\left(y \log(p) + (1 - y) \log(1 - p)\right). \tag{3}$$

The Dice loss is derived from the Dice Similarity Coefficient (DSC), which measures the overlap between predicted and true masks. With a smoothing constant ϵ to avoid division by zero, the DSC is defined as

$$DSC(y, p) \coloneqq \frac{2yp + \epsilon}{y + p + \epsilon},$$

and the Dice loss is computed as

$$\mathcal{L}_{Dice}(y, p) \coloneqq 1 - DSC(y, p). \tag{4}$$

The smoothing constant is usually set to $\epsilon = 1$ (Jadon 2020).

The proposed model is trained over 50 epochs using the loss function (2). We use Adam optimizer (Kingma 2014) with a learning rate of 10^{-4}.

3.4 Comparison Methods and Evaluation Metrics

We compare our model with the deep learning-based models UNet (Li et al. 2018), MANet (Fan et al. 2020), DUNet (Costa et al. 2024) and ResUNet. This last model is a modified UNet architecture whose details can be found in (PhiLab). All models were trained on the FloatingObject dataset. For each model, we used the same inputs as reported in their respective papers (when available): UNet, MANet and ResUNet were fed the S2 bands, while DUNet was additionally fed the NDVI and FDI indices.

For the quantitative comparison, we use the following metrics: Intersection over Union (IoU) (Jaccard 1901), which measures the overlap of correctly detected pixels and is widely used in segmentation tasks; Cohen's kappa index (κ) (Cohen 1960), which evaluates performance taking chance into account; and Dice Coefficient (Dice) (Dice 1945), which is similar to IoU but more sensitive to small objects. For all metrics, higher values indicate better performance, with a maximum score of 1.

4 Results

4.1 Quantitative and Qualitative results

Figure 4 presents the distribution of the IoU, κ, and Dice Score across all compared models. For each metric, boxplots grouped by model are shown, highlighting not only the differences in median but also the dispersion and presence of outliers. The proposed approach consistently exhibits higher median values and reduced variance compared to the other methods, indicating a more stable performance across all metrics.

Regarding the qualitative comparison, Figures 5, 6 and 7 display the RGB image to be segmented, the FDI and NDVI indices, the reference mask, and the resulting masks obtained by applying the input to all methods.

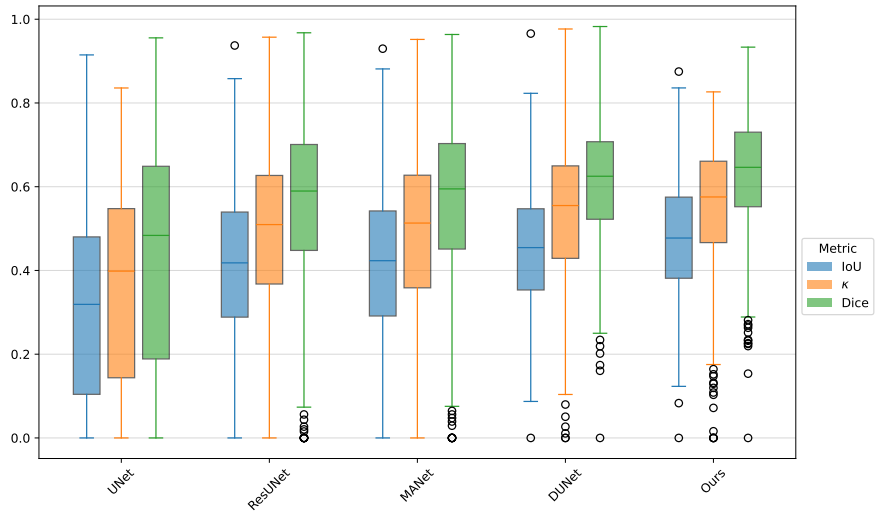

Fig. 4: Boxplot distribution of IoU, κ, and Dice scores for UNet, ResUNet, MANet, DUNet, and the proposed model, illustrating median performance and variability across samples. The proposed method provides higher median and reduced variance across all metrics.

In Figure 5, the masks produced by our model together with those generated by DUNet are the ones that most closely resemble the reference mask. However, in our case, the mask is more clearly defined and encompasses the majority of the target area, whereas DUNet provides a coarser result.

In Figure 6, the models that achieve the best segmentation of the objects are DUNet and our approach. Nevertheless, for the floating objects in the upper region, only our model is able to segment them. Moreover, our segmentation is considerably more sharply defined.

In Figure 7, DUNet, MANet, and our model successfully predict the line shape observed in the ground truth, whereas the other two models fail to do so. However, the lines produced by DUNet and MANet are noticeably thicker than the reference, while our model more accurately captures the true line thickness, resulting in fewer false positives.

In general, the poorest results are obtained with the UNet, as its simple encoder–decoder structure fails to effectively learn how to detect regions containing floating objects. In contrast, DUNet incorporates a more sophisticated design, with residual connections and an increasing number of feature channels, which leads to improved performance. Thanks to the addition of attention layers, our proposed TAUNet achieves the most accurate results, showing a considerable improvement over DUNet.

4.2 Ablation study

In this subsection, we evaluate the performance of the model under different parameter and architectural configurations. In particular, we assess whether guiding the network

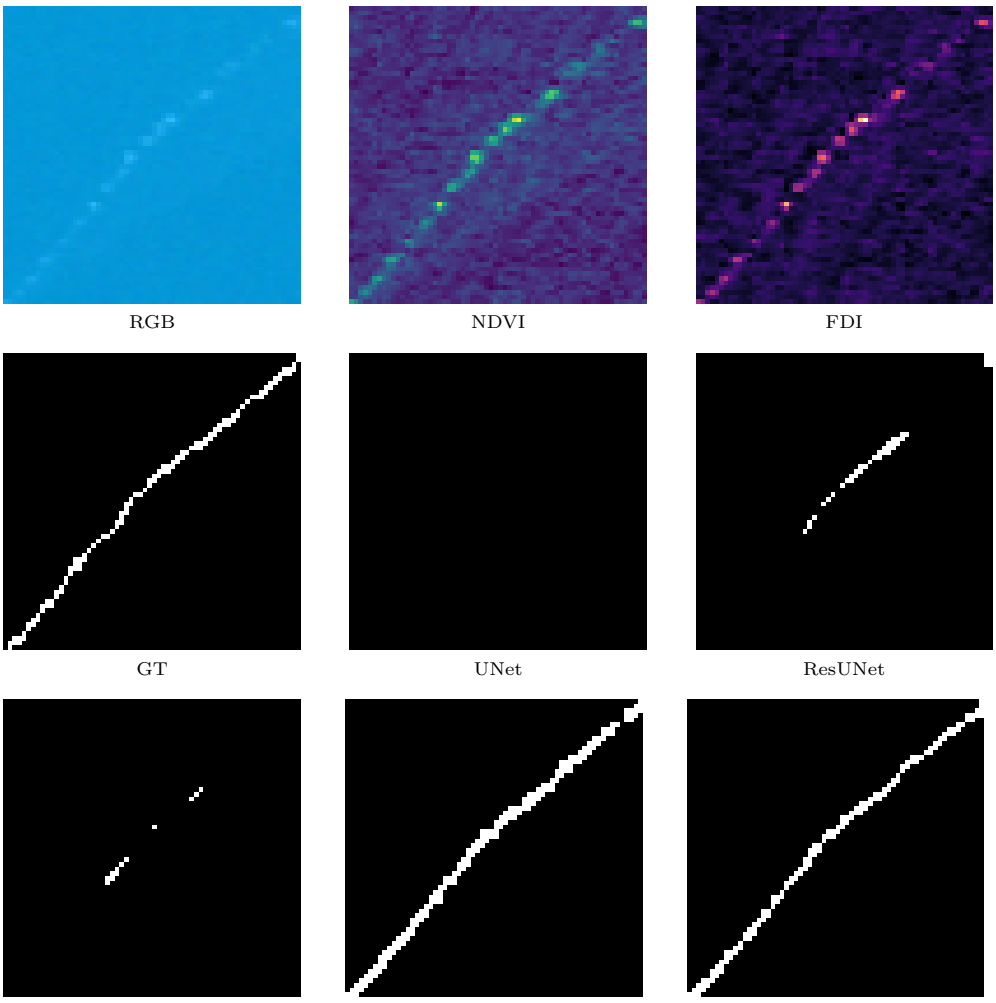

Fig. 5: Qualitative comparison of the marine litter segmentation networks on a crop extracted from the FloatingObjects dataset. The proposed approach provides the sharpest segmentation mask.

with the NDVI and FDI indices influences the results, the impact of the attention module architecture used in the decoder and the patch size employed by the transformer modules, the effect of varying the number of model features, and, finally, the choice of loss function.

Table 1 shows that incorporating the FDI and NDVI indices as inputs yields better results across all metrics than not incorporating them.

To enable the network to better capture relationships between different regions of the image within the feature maps, we introduce attention mechanisms in the decoder path. We study the impact of incorporating different architectures against

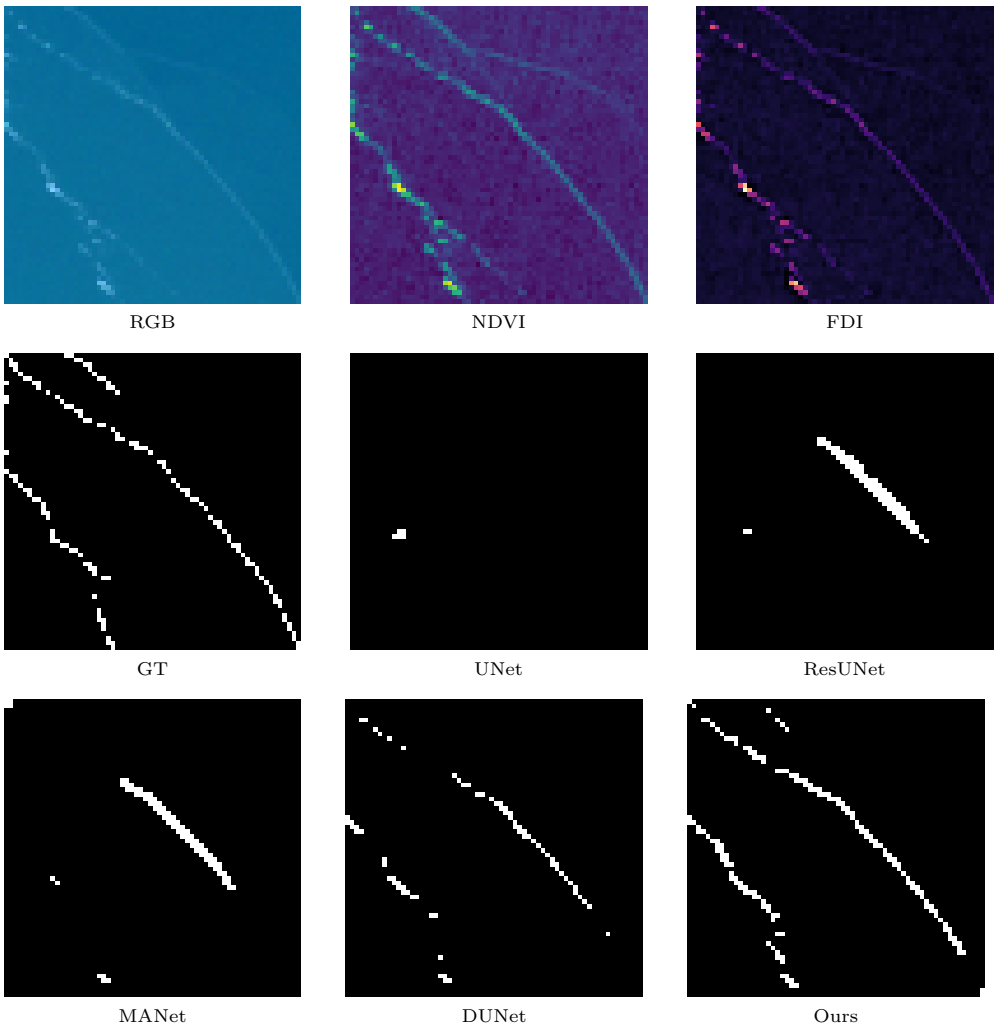

Fig. 6: Qualitative comparison of the marine litter segmentation networks on a crop extracted from the FloatingObjects dataset. Our prediction is the only one able to detect the floating objects in the top-center of the image.

our proposed Transformer Cross-Attention (TCA). Transformer Self-Attention (TSA) retains the full transformer structure, but applies only self-attention within each feature map. Self- and Cross-Attention (SCA) uses a simplified attention formulation without transformer components, directly applying self- or cross-attention on each decoder layer.

A quantitative comparison of the different attention modules is presented in Table 2, where it can be observed that the full transformer architecture using cross-attention outperforms the other variants. Qualitative-wise, as illustrated in Figure 8, the full transformer architecture using cross-attention also yields the best results, as the

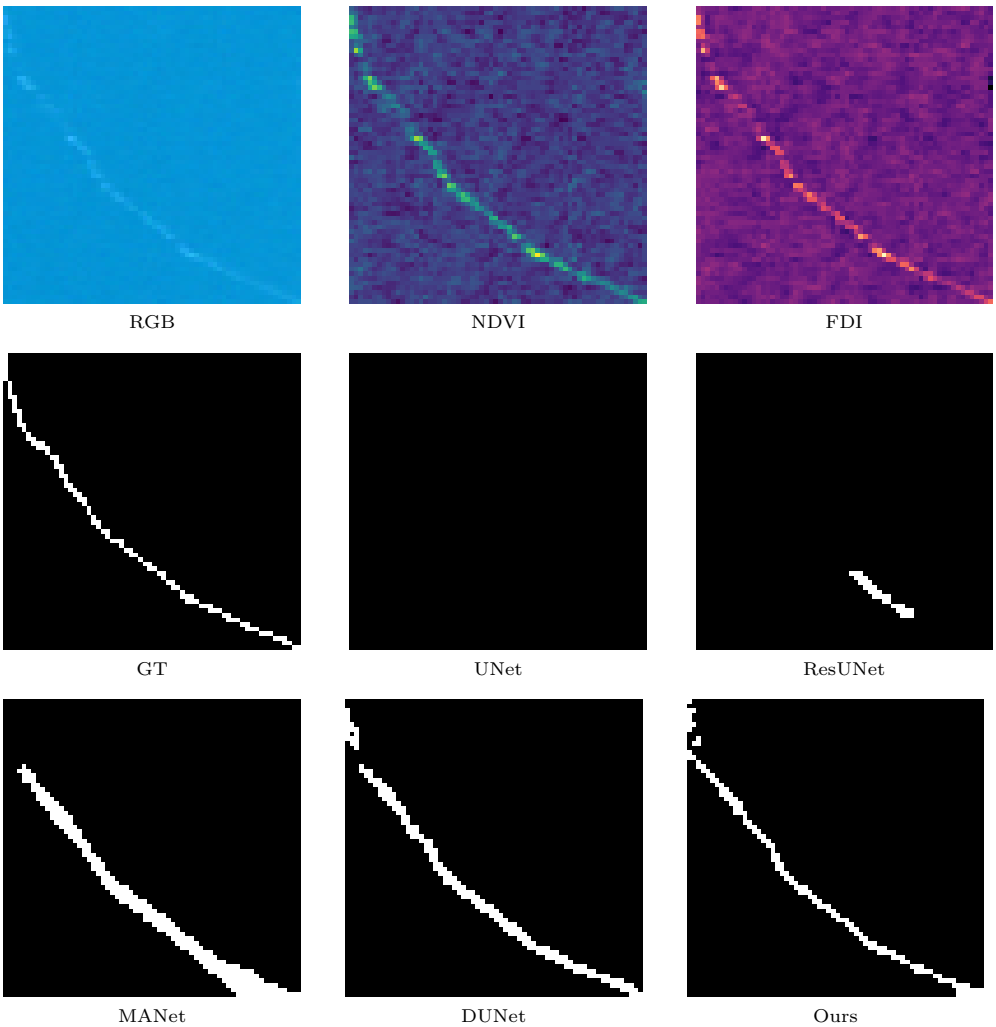

Fig. 7: Qualitative comparison of the marine litter segmentation networks on a crop extracted from the FloatingObjects dataset. DUNet, MANet, and our model successfully predict the line shape observed in the ground truth, with our model providing the most accurate thickness.

model using only self-attention generates a thicker line shape when compared to the ground truth, while the variant combining both self- and cross-attention results in a discontinuous line.

Applying attention mechanisms to the entire image would require each pixel to attend to every other pixel. Due to the resulting high computational complexity, we instead apply attention within blocks of varying sizes, following the approach of (Dosovitskiy 2020). In our case, we test patch sizes ranging from 1×1 to 8×8. The results in Table 3 show that the 1×1 patches yield the best performance.

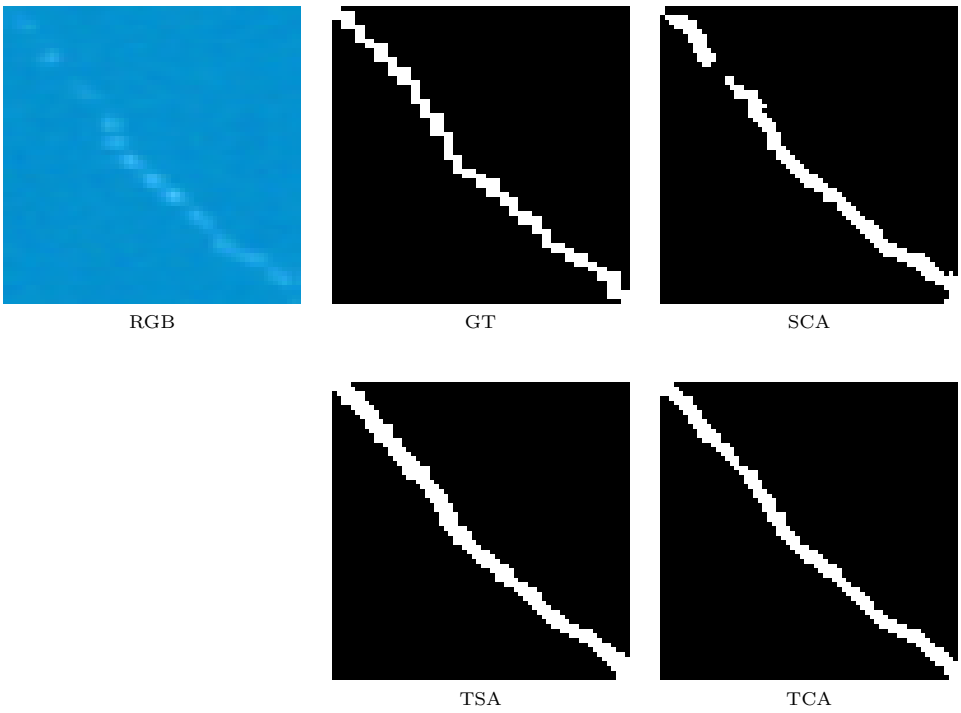

Fig. 8: Visual comparison of different architectures for the Transform layer in the Transformer Assisted UNet model. SCA denotes the architecture without transformer components which directly applies self- and cross-attention within each decoder layer; TSA includes only self-attention, and TCA represents our proposed cross-attention architecture. The cross-attention transformer provides the most accurate result, whereas self-attention produces thicker line shape and the combined version leads to fragmented lines.

To analyze the influence of the feature representation capacity on the network, we conduct an study on the number of hidden channels used throughout the architecture. We evaluate configurations with 32, 64, 128, and 248 hidden channels. As shown in Table 4, the best performance is achieved with 32 hidden channels.

To evaluate the suitability of the loss function, we compare the proposed loss (2) with the pure BCE loss (3) and the pure DICE loss (4). Table 5 shows the different performances, where we can observe that using the pure Dice loss slightly outperforms using the pure BCE loss across all metrics, while the proposed loss yields the best results across all metrics by a large margin.

5 Discussion

5.1 Model Performance

We performed a statistical significance analysis to determine whether our model significantly outperforms the competing models. Table 6 summarizes the results. Before

Table 1: Quantitative metrics for the full testing set for different sets of inputs. "No indices" corresponds to only using the S2 bands as inputs, and "FDI+NDVI" corresponds to additionally including the FDI and NDVI indices as inputs.

	IoU	κ	Dice
No indices	0.4454	0.5299	0.6240
FDI+NDVI	**0.4712**	**0.5315**	**0.6257**

Table 2: Quantitative comparison of the performance of different modules using: Self- and Cross-Attention (SCA), Transformer Self-Attention (TSA) and Transformer Cross-Attention (TCA). The best values are highlighted in bold.

	IoU	κ	Dice
SCA	0.4036	0.4709	0.5826
TSA	0.4355	0.5144	0.6138
TCA	**0.4712**	**0.5315**	**0.6257**

Table 3: Quantitative comparison of the performance of the model using different patch sizes on the transformer layers. The best values are highlighted in bold.

	IoU	κ	Dice
1	**0.4712**	**0.5315**	**0.6257**
2	0.4441	0.5276	0.6223
4	0.3512	0.3921	0.5279
8	0.2179	0.2488	0.3719

selecting the appropriate test, the normality of the sample distributions were evaluated. When both groups involved in a comparison satisfied the normality assumption (i.e., each model's distribution passed the Shapiro–Wilk test), the analysis was conducted using a one-sided Welch's t-test, which is suitable for parametric conditions and does not require equal variances. Conversely, when at least one of the groups did not satisfy the normality assumption, the non-parametric one-sided Mann–Whitney U test was used that does not rely on distributional assumptions. The table reports the selected statistical test and the corresponding p-value, and a significance mark indicates whether the target model outperforms the comparison model with $p < 0.05$.

Table 4: Quantitative comparison of the performance of the model using different number of features on the network. The best values are highlighted in bold.

	IoU	κ	Dice
32	**0.4712**	**0.5315**	**0.6257**
64	0.4359	0.5169	0.61471
128	0.4422	0.5256	0.6204
256	0.4424	0.5271	0.6208

Table 5: Quantitative comparison of the performance of the model using different loss functions. The best values are highlighted in bold.

	IoU	κ	Dice
BCE	0.4360	0.5193	0.6135
Dice	0.4402	0.5224	0.6176
BCE+Dice	**0.4712**	**0.5315**	**0.6257**

Overall, the results show that the performance improvements achieved by the proposed method are statistically significant for all metrics and model comparisons.

5.2 Impact of Index Usage

As seen in Table 1, considering the FDI and NDVI indices as additional inputs to our model leads to a better performance than not doing so, as all metrics are improved, specially the IoU. We attribute this improvement to the fact that these indices enhance the network's focus on the spectral bands most effective in distinguishing marine litter, thereby leading to a more reliable detection model.

We remark that, although the FDI and NDVI are the most widely used indices in the context of floating marine debris detection, several indices tailored to specific cases have also been considered in the literature (Sakti et al. 2023; Guffogg et al. 2024). As a potential direction for future work, an in-depth study could be made on the effectiveness of the aforementioned spectral indices at improving detection accuracy.

5.3 Impact of Network Architecture

About the Attention Module Variations, Self-attention helps model long-range dependencies within a single feature map, while cross-attention enhances the upsampled feature maps using information previously extracted by the encoder. Both attention blocks can be used to form transformer layers and establish global dependencies between the input and the output.

The superiority of the transformer-based layers is evident in Table 2 and Figure 8. Moreover, the performance obtained when considering only self-attention is slightly

Metric	Ours vs.	Statistical Test	p-value	Significant (✓/×)
mIoU	MANet	Mann–Whitney U	1.37e-09	✓
	DUNet	Welch t-test	7.59e-03	✓
	UNet	Mann–Whitney U	2.92e-41	✓
	ResUNet	Mann–Whitney U	6.97e-11	✓
κ	MANet	Mann–Whitney U	1.95e-10	✓
	DUNet	Mann–Whitney U	6.47e-03	✓
	UNet	Mann–Whitney U	2.31e-50	✓
	ResUNet	Mann–Whitney U	4.32e-13	✓
Dice	MANet	Mann–Whitney U	1.37e-09	✓
	DUNet	Mann–Whitney U	5.53e-03	✓
	UNet	Mann–Whitney U	2.92e-41	✓
	ResUNet	Mann–Whitney U	6.97e-11	✓

Table 6: Statistical significance analysis comparing the performance of the proposed model against the other models for each metric. Normality of the score distributions was assessed using the Shapiro–Wilk test; when both groups satisfied this assumption, a one-sided Welch's t-test was applied, otherwise a one-sided Mann–Whitney U test was used. The table lists the selected test, the corresponding p-value, and whether the difference is statistically significant at the $p < 0.05$ threshold.

lower, as no external reference beyond the feature map itself is available to serve as keys and queries. Therefore, we can conclude that integrating attention layers into the basic UNet architecture yields a meaningful improvement in detection performance.

Another important aspect of attention-based architectures is the size of the blocks over which the attention mechanism is applied. As shown in Table 3, pixel-level attention proves more effective during the upsampling stages of the network, which are crucial for restoring spatial detail in segmentation tasks.

Additionally, in Table 4 we study the optimal number of features in the network. Increasing the number of features generally leads to richer feature representations but also results in a potential overfitting for larger values. These results indicate that a moderate feature dimensionality provides an optimal balance.

As seen in Table 5, the pure BCE and pure Dice loss give comparable results, with the latter slightly outperforming the former. We can argue that this is due to the fact that the FloatingObjects dataset has significantly more pixels labeled as nonfloating objects than labeled as floating objects, and the BCE loss is more sensitive to imbalanced datasets than the Dice loss. That being said, the Dice loss itself is known to be sensitive to small objects, which are also present in the dataset. In any case, leveraging both losses yields the best results, which we attribute to each loss compensating for the other's weaknesses.

5.4 Extension to a Full Detection Pipeline

Our model has been trained on the FloatingObjects dataset, which provides S2 images with all spectral bands pre-upscaled to a 10 m resolution. Our model could be extended to a full marine litter detection pipeline by incorporating a satellite image fusion

procedure prior to the detection network. This would enable the model to work on raw S2 products, which would provide a more complete end-to-end model that does not rely on preprocessed S2 data.

5.5 Limitations of the Study

The coarse spatial resolution satellite imagery, the scarcity of readily available datasets and the inherent class imbalance makes satellite-based floating marine litter detection a challenging task. Although TAUNet demonstrates qualitative and quantitative improvements over recently proposed models, the overall performance metrics remain modest. Furthermore, the dataset we have used is of relative small size, which limits the model's ability to generalize to unseen scenes. Moreover, our model is only able to detect general marine debris, as the training dataset only distinguishes floating objects pixels from non-floating object pixels. Consequently, our model serves as a preliminary procedure to detect areas which are likely to contain plastic. Ultimately, while fully automated plastic detection using satellite imagery is still a distant goal, our work represents a meaningful step toward this objective, though substantial further advances are still required.

6 Conclusions

In this article, we have presented a novel marine litter detection model using S2 imagery, which extends the DUNet model (Costa et al. 2024) by introducing attention mechanisms into the decoder, resulting in a significant improvement. Specifically, we have incorporated a transformer layer in which self-attention is employed at the lowest level, while cross-attention is applied at subsequent levels using the corresponding encoder outputs to compute the attention maps. A comparative evaluation against several state-of-the-art models have demonstrated the superiority of our approach both quantitatively and qualitatively.

Moreover, several aspects of the model have been tested in order to obtain the best performing combination. In particular, we have demonstrated that, as suggested by prior literature, including the FDI and NDVI spectral indices as additional inputs reduces vegetation-related confusion and improves overall detection accuracy.

Nonetheless, we acknowledge various limitations. Despite the dataset used presenting substantial variability, its size is relatively small. Moreover, our model is only capable of detecting generic marine debris and cannot discriminate plastic from other forms of floating litter. Our model only works on S2 data whose bands has been upscaled to 10 m, and cannot operate on unprocessed products.

Overall, this study serves as an advancement towards automated satellite-based marine plastic detection. It significantly improves the current state of the art approaches and highlights the potential of deep learning-based techniques for addressing this pressing environmental challenge.

Acknowledgements

This work was funded by MICIU/AEI/10.13039/501100011033 and by the European Union NextGenerationEU/PRTR via MaLiSat project TED2021-132644B-I00, and also by MCIN/AEI/10.13039/501100011033 and "ERDF A way of making Europe" through European Union under Grant PID2021-125711OB-I00. Ivan Pereira-Sánchez is grateful for the funding provided by the Conselleria de Fons Europeus, Universitat i Cultura (GOIB) under grant FPU2023-004-C. Daniel Torres is grateful for the funding provided by the Conselleria d'Educació i Universitats (GOIB) under grant FPU2024-002-C. Bartomeu Garau is grateful for the funding provided by the Conselleria d'Educació i Universitats (GOIB) under grant FPU2025-008-C. The authors gratefully acknowledge the computer resources at Artemisa, funded by the EU ERDF and Comunitat Valenciana and the technical support provided by IFIC (CSIC-UV).

References

Andrady, A.L.: Persistence of plastic litter in the oceans. In: Marine Anthropogenic Litter, pp. 57–72. Springer, Cham (2015)

Aretoulaki, E., Ponis, S., Plakas, G., Agalianos, K., *et al.*: Marine plastic littering: A review of socio economic impacts. J. Sustain. Sci. Manag **16**(3), 277–301 (2021)

Biermann, L., Clewley, D., Martinez-Vicente, V., Topouzelis, K.: Finding plastic patches in coastal waters using optical satellite data. Scientific reports **10**(1), 5364 (2020)

Ben Salah, K., Othmani, M., Fourati, J., Kherallah, M.: Advancing spatial mapping for satellite image road segmentation with multi-head attention. The Visual Computer **41**(4), 2079–2089 (2025)

Basu, B., Sannigrahi, S., Sarkar Basu, A., Pilla, F.: Development of novel classification algorithms for detection of floating plastic debris in coastal waterbodies using multispectral sentinel-2 remote sensing imagery. Remote Sensing **13**(8), 1598 (2021)

Ciappa, A.C.: Marine plastic litter detection offshore hawai'i by sentinel-2. Marine Pollution Bulletin **168**, 112457 (2021)

Cui, M., Li, K., Chen, J., Yu, W.: Cm-unet: A novel remote sensing image segmentation method based on improved u-net. IEEE Access **11**, 56994–57005 (2023)

Carmo, R., Mifdal, J., Rußwurm, M.: Detecting macro floating objects on coastal water bodies using sentinel-2 data. In: OCEANS 2021: San Diego–Porto, pp. 1–7 (2021). IEEE

Cheng, B., Misra, I., Schwing, A.G., Kirillov, A., Girdhar, R.: Masked-attention mask transformer for universal image segmentation. In: Proceedings of the IEEE/CVF Conference on Computer Vision and Pattern Recognition, pp. 1290–1299 (2022)

Cohen, J.: A coefficient of agreement for nominal scales. Educational and psychological measurement **20**(1), 37–46 (1960)

Chen, L.-C., Papandreou, G., Schroff, F., Adam, H.: Rethinking atrous convolution for semantic image segmentation. arXiv preprint arXiv:1706.05587 (2017)

Carlson, D.F., Suaria, G., Aliani, S., Fredj, E., Fortibuoni, T., Griffa, A., Russo, A., Melli, V.: Combining litter observations with a regional ocean model to identify sources and sinks of floating debris in a semi-enclosed basin: the adriatic sea. Frontiers in Marine Science **4**, 78 (2017)

Costa, A., Sans, E., Pereira-Sánchez, I., Duran, J., Navarro, J.: Improving marine litter segmentation with limited resolution satellite imagery. In: 2024 International Conference on Machine Intelligence for GeoAnalytics and Remote Sensing (MIGARS), pp. 1–3 (2024). IEEE

Dice, L.R.: Measures of the amount of ecologic association between species. Ecology **26**(3), 297–302 (1945)

Dosovitskiy, A.: An image is worth 16x16 words: Transformers for image recognition at scale. arXiv preprint arXiv:2010.11929 (2020)

De Vries, R., Egger, M., Mani, T., Lebreton, L.: Quantifying floating plastic debris at sea using vessel-based optical data and artificial intelligence. Remote Sensing **13**(17), 3401 (2021)

Escobar-Sánchez, G., Markfort, G., Berghald, M., Ritzenhofen, L., Schernewski, G.: Aerial and underwater drones for marine litter monitoring in shallow coastal waters: factors influencing item detection and cost-efficiency. Environmental monitoring and assessment **194**(12), 863 (2022)

European Space Agency: Sentinel-2 — SentiWiki. https://sentiwiki.copernicus.eu/web/sentinel-2. Accessed: 2025-05-16 (2025)

Fan, T., Wang, G., Li, Y., Wang, H.: Ma-net: A multi-scale attention network for liver and tumor segmentation. Ieee Access **8**, 179656–179665 (2020)

Galgani, F., Brien, A.S.-o., Weis, J., Ioakeimidis, C., Schuyler, Q., Makarenko, I., Griffiths, H., Bondareff, J., Vethaak, D., Deidun, A., *et al.*: Are litter, plastic and microplastic quantities increasing in the ocean? Microplastics and Nanoplastics **1**(1), 2 (2021)

Galgani, F., Hanke, G., Maes, T.: Global distribution, composition and abundance of marine litter. In: Marine Anthropogenic Litter, pp. 29–56. Springer, Cham (2015)

Guffogg, J., Soto-Berelov, M., Bellman, C., Jones, S., Skidmore, A.: Beached plastic debris index; a modern index for detecting plastics on beaches. Marine Pollution

Bulletin **209**, 117124 (2024)

Gómez, À.S., Scandolo, L., Eisemann, E.: A learning approach for river debris detection. International Journal of Applied Earth Observation and Geoinformation **107**, 102682 (2022)

Ioffe, S., Szegedy, C.: Batch normalization: Accelerating deep network training by reducing internal covariate shift. In: International Conference on Machine Learning, pp. 448–456 (2015). pmlr

Jaccard, P.: Étude comparative de la distribution florale dans une portion des alpes et des jura. Bull Soc Vaudoise Sci Nat **37**, 547–579 (1901)

Jadon, S.: A survey of loss functions for semantic segmentation. In: 2020 IEEE Conference on Computational Intelligence in Bioinformatics and Computational Biology (CIBCB), pp. 1–7 (2020). IEEE

Jamali, A., Mahdianpari, M.: A cloud-based framework for large-scale monitoring of ocean plastics using multi-spectral satellite imagery and generative adversarial network. Water **13**(18), 2553 (2021)

Kingma, D.P.: Adam: A method for stochastic optimization. arXiv preprint arXiv:1412.6980 (2014)

Kikaki, K., Kakogeorgiou, I., Hoteit, I., Karantzalos, K.: Detecting marine pollutants and sea surface features with deep learning in sentinel-2 imagery. ISPRS Journal of Photogrammetry and Remote Sensing **210**, 39–54 (2024)

Kikaki, K., Kakogeorgiou, I., Mikeli, P., Raitsos, D.E., Karantzalos, K.: Marida: A benchmark for marine debris detection from sentinel-2 remote sensing data. PloS one **17**(1), 0262247 (2022)

Liu, Y., Bai, X., Wang, J., Li, G., Li, J., Lv, Z.: Image semantic segmentation approach based on deeplabv3 plus network with an attention mechanism. Engineering Applications of Artificial Intelligence **127**, 107260 (2024)

Liu, G., Diao, K., Zhu, J., Wang, Q., Li, M.: Stransu2net: Transformer based hybrid model for building segmentation in detailed satellite imagery. PloS one **19**(9), 0299732 (2024)

Li, R., Liu, W., Yang, L., Sun, S., Hu, W., Zhang, F., Li, W.: Deepunet: A deep fully convolutional network for pixel-level sea-land segmentation. IEEE journal of selected topics in applied earth observations and remote sensing **11**(11), 3954–3962 (2018)

Li, H., Qiu, K., Chen, L., Mei, X., Hong, L., Tao, C.: Scattnet: Semantic segmentation network with spatial and channel attention mechanism for high-resolution remote

sensing images. IEEE Geoscience and Remote Sensing Letters **18**(5), 905–909 (2020)

Löhr, A., Savelli, H., Beunen, R., Kalz, M., Ragas, A., Van Belleghem, F.: Solutions for global marine litter pollution. Current opinion in environmental sustainability **28**, 90–99 (2017)

Mafuta, C., Baker, E., Rucevska, I., Thygesen, K., Appelquist, L.R., Westerveld, L., Tsakona, M., Macmillan-Lawler, M., Harris, P., Sevaldsen, P., et al.: Drowning in plastics: marine litter and plastic waste vital graphics. ¡ bound method Organization. get_name_with_acronym of¡ Organization: Grid ... (2021)

Morales-Caselles, C., Viejo, J., Martí, E., González-Fernández, D., Pragnell-Raasch, H., González-Gordillo, J., Montero, E., Arroyo, G., Hanke, G., Salvo, V., et al.: An inshore–offshore sorting system revealed from global classification of ocean litter. Nat. Sustain. 4, 484–493 (2021)

Mansui, J., Darmon, G., Ballerini, T., Canneyt, O., Ourmières, Y., Miaud, C.: Predicting marine litter accumulation patterns in the mediterranean basin: Spatio-temporal variability and comparison with empirical data. Progress in Oceanography **182**, 102268 (2020)

Mifdal, J., Longépé, N., Rußwurm, M.: Towards detecting floating objects on a global scale with learned spatial features using sentinel 2. ISPRS Annals of the Photogrammetry, Remote Sensing and Spatial Information Sciences **3**, 285–293 (2021)

Merlino, S., Paterni, M., Berton, A., Massetti, L.: Unmanned aerial vehicles for debris survey in coastal areas: Long-term monitoring programme to study spatial and temporal accumulation of the dynamics of beached marine litter. Remote Sensing **12**(8), 1260 (2020)

Merlino, S., Paterni, M., Locritani, M., Andriolo, U., Gonçalves, G., Massetti, L.: Citizen science for marine litter detection and classification on unmanned aerial vehicle images. Water **13**(23), 3349 (2021)

McIlgorm, A., Raubenheimer, K., McIlgorm, D.E., Nichols, R.: The cost of marine litter damage to the global marine economy: Insights from the asia-pacific into prevention and the cost of inaction. Marine Pollution Bulletin **174**, 113167 (2022)

Nivedita, V., Begum, S.S., Aldehim, G., Alashjaee, A.M., Arasi, M.A., Sikkandar, M.Y., Jayasankar, T., Vivek, S.: Plastic debris detection along coastal waters using sentinel-2 satellite data and machine learning techniques. Marine Pollution Bulletin **209**, 117106 (2024)

Park, Y.-J., Garaba, S.P., Sainte-Rose, B.: Detecting the great pacific garbage patch floating plastic litter using worldview-3 satellite imagery. Optics Express **29**(22),

35288–35298 (2021)

PhiLab, E.: FloatingObjects. https://github.com/ESA-PhiLab/floatingobjects. GitHub repository. Accessed: 2025-09-30

Rußwurm, M., Venkatesa, S.J., Tuia, D.: Large-scale detection of marine debris in coastal areas with sentinel-2. iScience **26**(12) (2023)

Ruan, J., Xiang, S., Xie, M., Liu, T., Fu, Y.: Malunet: A multi-attention and light-weight unet for skin lesion segmentation. In: 2022 IEEE International Conference on Bioinformatics and Biomedicine (BIBM), pp. 1150–1156 (2022). IEEE

Sannigrahi, S., Basu, B., Basu, A.S., Pilla, F.: Development of automated marine floating plastic detection system using sentinel-2 imagery and machine learning models. Marine Pollution Bulletin **178**, 113527 (2022)

Salgado-Hernanz, P.M., Bauzà, J., Alomar, C., Compa, M., Romero, L., Deudero, S.: Assessment of marine litter through remote sensing: recent approaches and future goals. Marine Pollution Bulletin **168**, 112347 (2021)

Soto-Navarro, J., Jordá, G., Compa, M., Alomar, C., Fossi, M.C., Deudero, S.: Impact of the marine litter pollution on the mediterranean biodiversity: A risk assessment study with focus on the marine protected areas. Marine Pollution Bulletin **165**, 112169 (2021)

Sakti, A.D., Sembiring, E., Rohayani, P., Fauzan, K.N., Anggraini, T.S., Santoso, C., Patricia, V.A., Ihsan, K.T.N., Ramadan, A.H., Arjasakusuma, S., *et al.*: Identification of illegally dumped plastic waste in a highly polluted river in indonesia using sentinel-2 satellite imagery. Scientific Reports **13**(1), 5039 (2023)

Taggio, N., Aiello, A., Ceriola, G., Kremezi, M., Kristollari, V., Kolokoussis, P., Karathanassi, V., Barbone, E.: A combination of machine learning algorithms for marine plastic litter detection exploiting hyperspectral prisma data. Remote Sensing **14**(15), 3606 (2022)

Topouzelis, K., Papakonstantinou, A., Garaba, S.P.: Detection of floating plastics from satellite and unmanned aerial systems (plastic litter project 2018). International Journal of Applied Earth Observation and Geoinformation **79**, 175–183 (2019)

Topouzelis, K., Papageorgiou, D., Karagaitanakis, A., Papakonstantinou, A., Arias Ballesteros, M.: Remote sensing of sea surface artificial floating plastic targets with sentinel-2 and unmanned aerial systems (plastic litter project 2019). Remote Sensing **12**(12), 2013 (2020)

Themistocleous, K., Papoutsa, C., Michaelides, S., Hadjimitsis, D.: Investigating detection of floating plastic litter from space using sentinel-2 imagery. Remote Sensing **12**(16), 2648 (2020)

Topouzelis, K., Papageorgiou, D., Suaria, G., Aliani, S.: Floating marine litter detection algorithms and techniques using optical remote sensing data: A review. Marine Pollution Bulletin **170**, 112675 (2021)

Vaswani, A., Shazeer, N., Parmar, N., Uszkoreit, J., Jones, L., Gomez, A.N., Kaiser, Ł., Polosukhin, I.: Attention is all you need. Advances in neural information processing systems **30** (2017)

Wayman, C., Niemann, H.: The fate of plastic in the ocean environment–a minireview. Environmental Science: Processes & Impacts **23**(2), 198–212 (2021)

Woods, J.S., Verones, F., Jolliet, O., Vázquez-Rowe, I., Boulay, A.-M.: A framework for the assessment of marine litter impacts in life cycle impact assessment. Ecological Indicators **129**, 107918 (2021)

Yang, R., Uchida, K., Miyamoto, Y., Arakawa, H., Hagita, R., Aikawa, T.: Development of a ship-based camera monitoring system for floating marine debris. Marine Pollution Bulletin **206**, 116722 (2024)

Zhao, G., Zhang, Y., Ge, M., Yu, M.: Bilateral u-net semantic segmentation with spatial attention mechanism. CAAI Transactions on Intelligence Technology **8**(2), 297–307 (2023)